

Zeeman tunability of Andreev bound states in van-der-Waals tunnel barriers

Tom Dvir,[†] Marco Aprili,[‡] Charis H. L. Quay,[‡] and Hadar Steinberg[†]

[†]*The Racah Institute of Physics, The Hebrew University of Jerusalem, Givat Ram,
Jerusalem 91904 Israel*

[‡]*Laboratoire de Physique des Solides (CNRS UMR 8502), Batiment 510, Universite
Paris-Sud/Universite Paris-Saclay, 91405 Orsay, France*

E-mail:

Abstract

Quantum dots proximity-coupled to superconductors are attractive research platforms due to the intricate interplay between the single-electron nature of the dot and the many body nature of the superconducting state. These have been studied mostly using nanowires and carbon nanotubes, which allow a combination of tunability and proximity. Here we report a new type of quantum dot which allows proximity to a broad range of superconducting systems. The dots are realized as embedded defects within semiconducting tunnel barriers in van-der-Waals layers. By placing such layers on top of thin NbSe₂, we can probe the Andreev bound state spectra of such dots up to high in-plane magnetic fields without observing effects of a diminishing superconducting gap. As tunnel junctions defined on NbSe₂ have a hard gap, we can map the sub-gap spectra without background related to the rest of the junction. We find that the proximitized defect states invariably have a singlet ground state, manifest in the Zeeman splitting of the sub-gap excitation. We also find, in some cases, bound states which converge to zero energy and remain there. We discuss the role of the spin-orbit

term, present both in the barrier and the superconductor, in the realization of such topologically trivial zero-energy states.

Keywords

Tunneling, NbSe₂

Introduction

In a quantum dot (QD) residing at close proximity to a superconductor, the excitation spectrum is governed by an interplay between induced superconductivity, charging energy, and chemical potential. Such coupling was initially studied by integrating dots into Josephson junctions ('S-QD-S' Devices) which may be studied in the strong or weak coupling regime.¹ In the alternative 'N-QD-S' geometry, sub-gap energies are probed directly. Here, the dot is weakly coupled to a normal electrode on one side, and strongly coupled to a superconductor on the other. Charge transfer through the dot and into the superconductor is carried through Andreev processes involving transitions between the ground and excited states.¹⁻⁵ These transition energies appear as features in the tunneling spectra, below the superconducting gap Δ . 'N-QD-S' systems were realized by evaporating contacts on top of carbon nanotubes,^{6,7} self-assembled dots,⁸ and semiconducting nanowires (NWs).^{9,10} These systems allow for gate-tunability of the dot chemical potential, generating a transition between two distinct ground states: An even parity, Cooper-pair-like singlet, and an odd parity, single-electron doublet.^{4,9-12} Tuning the ground state into the doublet ground state is also possible by the application of in-plane magnetic field. In this case, the doublet state energy is Zeeman split, with the lower energy branch crossing the singlet energy at a finite applied field.⁹

In recent years, a major research drive is aimed at probing the spectra of Majorana excitations, predicted to appear and observed as a zero-bias spectral feature in NWs proximity

coupled to superconductors.¹³⁻¹⁷ Following these works, it became apparent that dots coupled to superconductors can also exhibit a peak similar to the expected Majorana signal at near zero energies. This happens when the dot is characterized by a strong spin-orbit coupling (SOC) term.¹⁸⁻²⁰ More generally, understanding how the ABS spectrum develops at the presence of a SO term is important for distinguishing between trivial and topological states.

A trivial system can exhibit a zero-energy spectral feature when the lower spin branch of the Zeeman split doublet state becomes degenerate with the singlet. Observing this crossover is an experimental challenge: It requires the energy scale $g\mu_B H$ (where g is the Landé g factor, μ_B is the Bohr magneton and H is the magnitude of the field) to become significant while the superconductor retains a finite gap. To observe such splitting, some studies employed materials with a high g factor,⁹ although results might be obscured by the diminishing of Δ with H . Here we use an alternative - to couple a quantum dot to an ultrathin superconductor - such as NbSe₂. NbSe₂ is a van-der-Waals superconductor, which remains superconducting at the ultrathin limit. Coupling QDs to NbSe₂ has two advantages: First, the superconducting gap of ultrathin NbSe₂ experiences very little change up to fields of a few Tesla in the plane.²¹ Second, NbSe₂ and related transition metal dichalcogenide (TMD) materials are characterized by strong Ising SO coupling. It is of interest to consider the role of such SO terms on proximitized dot spectra.

In this work we fabricate and measure tunnel devices consisting of TMD barriers placed on top of NbSe₂, as reported in our earlier works.^{21,22} The tunneling spectra exhibit Andreev bound states formed in naturally occurring quantum dots in the barrier. The spectra undergo clear Zeeman splitting at the presence of in-plane magnetic field, and are tracked up to 9 T. The majority of dots studied exhibit continuous spectral evolution, with a singlet to doublet crossover at some finite field. In some cases, however, we find a field-dependent transition to zero energy peaks. We suggest these are of trivial topology, and discuss their possible origin.

Results

Observation of subgap states

Figure 1a shows a sketch of the devices reported in this work. Normal - insulator - superconductor (NIS) tunnel junctions were fabricated using the dry transfer technique, by placing a few layer semiconductor TMD (WSe₂) on top of a flake of 2H-NbSe₂ (NbSe₂) of thickness ranging between 2 and 50 nm. Normal counter electrodes were fabricated using standard e-beam lithography methods as reported earlier.²² Typical junction dimensions are in the order of 1-2 μm^2 and barriers are 2-3 nm thick. Measurements are conducted using standard lock-in technique, where a bias voltage V is applied to the Au counter electrode and the current I and differential conductance dI/dV are measured through a current pre-amp in ohmic contact with the NbSe₂ bulk. Measurements were conducted at base temperature below 70 mK, with AC excitation in the range of 20-50 μeV .

The problem of a quantum dot that is coupled to a superconductor and to a normal metal is usually formulated in terms of the Anderson impurity model. This model accounts for tunneling between the dot and respective electrodes, and for the on-site electrostatic repulsion on the dot. The full solution of the model requires sophisticated computational tools and is beyond the scope of this paper. However we gain sufficient intuition by considering the case of a ‘superconducting impurity’:^{4,23} when the coupling of the the superconducting electrode Γ_S is much larger than the coupling to the normal electrode Γ_N and the intrinsic superconducting gap Δ is the largest parameter in the system, an effective on-site interaction forms on the dot whose magnitude equals $\Delta_d = \Gamma_S/2$. The effective Hamiltonian then reads:

$$H_{QD} = \sum_{\sigma} E_0 d_{\sigma}^{\dagger} d_{\sigma} - \frac{\Gamma_s}{2} \left(d_{\downarrow}^{\dagger} d_{\uparrow}^{\dagger} + h.c. \right) + U n_{d\downarrow} n_{d\uparrow} \quad (1)$$

where E_0 is the energy level of the dot, $d_{\sigma}^{\dagger}, d_{\sigma}$ are the creation and annihilation operators for spin σ , $n_{\sigma} = d_{\sigma}^{\dagger} d_{\sigma}$ is the number operator for spin σ , and U is the electrostatic repul-

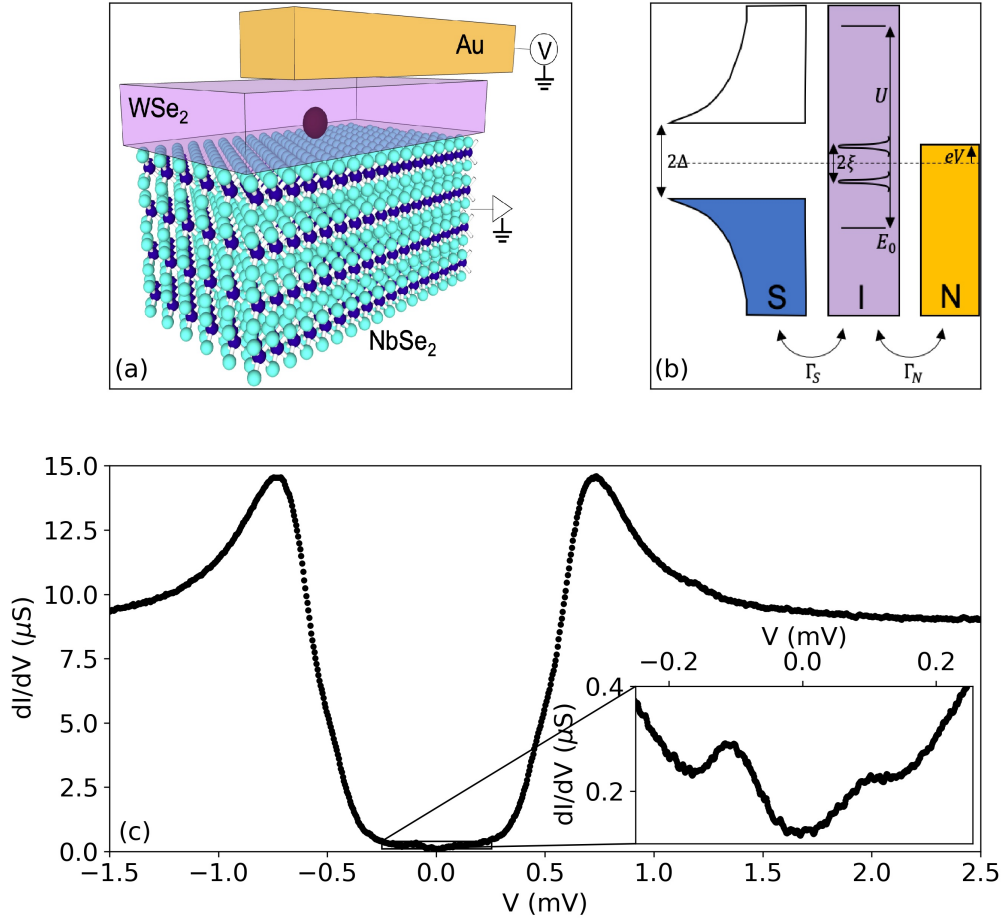


Figure 1: **Sub gap states in van der Waals tunnel junctions:** **a.** Device schematics: a layer of NbSe₂ is connected to the ground and is covered by a thin barrier in which a quantum dot is formed. Ti/Au electrode is evaporated above and connected to a voltage source. **b.** Schematic model for tunneling between a superconductor to a normal metal through a quantum dot. Details in main text. **c.** Differential conductance of Device 1 at base temperature at zero magnetic field. Inset: magnification of the sub-gap region showing the two Andreev peaks formed symmetrically around zero.

sion energy of the dot, as depicted in the scheme shown in figure 1b. Diagonalization of this Hamiltonian is straight-forward: There are two degenerate doublet eigenstates, $|\uparrow\rangle$, $|\downarrow\rangle$ with the energy E_0 and two ‘singlet’ eigenstates which consist of the superposition of zero occupancy state, $|0\rangle$, and the double occupancy state, $|\uparrow\downarrow\rangle$:

$$|\Psi_-\rangle = u_d |0\rangle - v_d |\uparrow\downarrow\rangle \quad (2)$$

$$|\Psi_+\rangle = v_d |0\rangle + u_d |\uparrow\downarrow\rangle \quad (3)$$

$$E_{\pm} = \left(E_0 + \frac{U}{2}\right) \pm \sqrt{\left(E_0 + \frac{U}{2}\right)^2 + \left(\frac{\Gamma_s}{2}\right)^2} \quad (4)$$

The ground state of the system can be either the doublet or Ψ_- , depending on the interplay between U , E_0 and Γ_s . Tunneling experiments probe the energies corresponding to transitions where the number of electrons in the system is changed by one. In superconducting dots this process requires a transition between singlet and doublet states, with the energies: $\pm\xi = \frac{U}{2} - \sqrt{\left(E_0 + \frac{U}{2}\right)^2 + \left(\frac{\Gamma_s}{2}\right)^2}$. While the simplified picture presented here is correct only in the limit of large superconducting gap, and doesn’t take into account Kondo correlations, we believe that it qualitatively accounts for the observed data.

Figure 1c shows the differential conductance as measured with Device 1. The observed density of states shows a clear superconducting gap with quasi-particle peaks at energies of $\approx 800\mu\text{V}$ as discussed elsewhere.²¹ The sub-gap spectrum shows two peaks with energies of $\approx 100\mu\text{V}$ above a parabolic background. Such sub-gap peaks, observed in many of the tunnel junctions fabricated, are the subject of this report, and represent the singlet to doublet transition energy ξ .

Magnetic field dependence

An important knob for the control and study of dot-bound states is magnetic field. Application of field lifts the degeneracy between the two doublet states, with a Zeeman energy

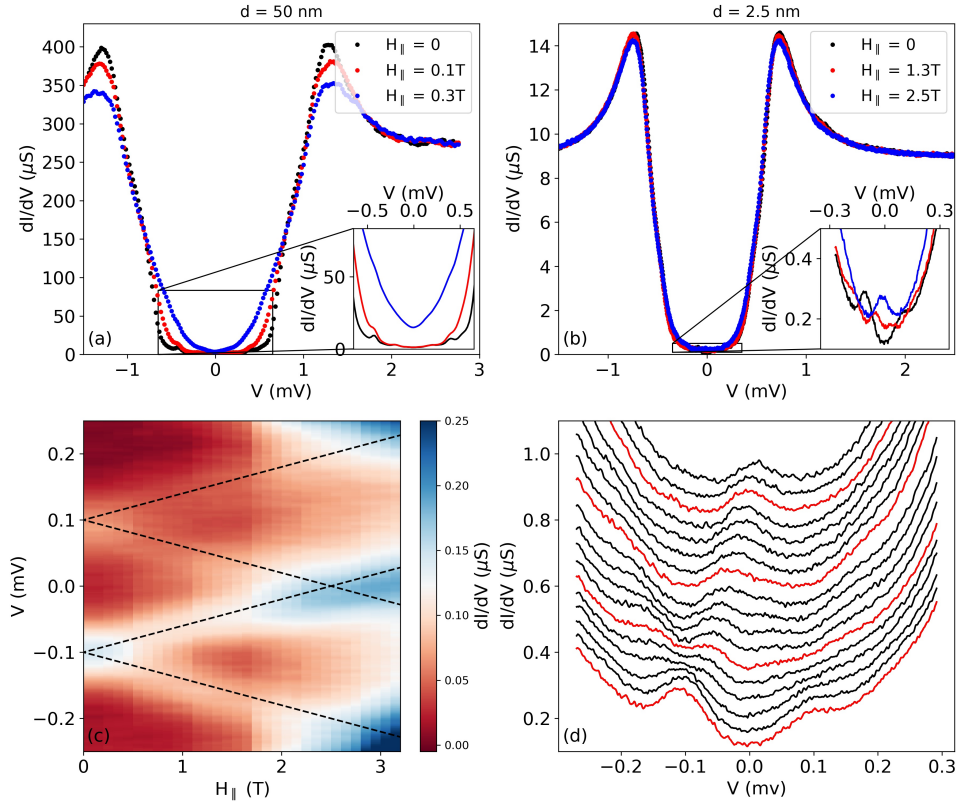


Figure 2: **Sub gap states in van der Waals tunnel junctions:** **a.,b.** Differential conductance of Device 2 (50 nm thick) and Device 1 (2.5 nm thick) at increasing in-plane magnetic field. **Insets:** zoom in on the sub-gap spectrum. **c.** Color map of the sub-gap conductance of Device 1 with increasing in-plane magnetic field. Dotted black lines trace the evolution of the sub-gap peaks with a slope of $40 \mu\text{eV}/\text{T}$, equivalent to a g factor of 1.3. **d.** Shifted differential conductance curves from the sub-gap region of Device 2, the curves are shown at intervals of 0.2 T. Red curves are shown at intervals of 1 T.

$E_z = \pm g\mu_B H$. Lifting of the doublet degeneracy allows the distinction between a singlet and a doublet ground state. When the ground-state is a doublet, application of field shifts its energy downwards, increasing the doublet-singlet energy difference and thus merely increasing the observed excitation energy. If, however, the ground-state is the singlet state, the excitation energy splits, eventually leading to a cross-over when the Zeeman energy equals ξ . Figure 2a shows the spectrum of Device 2 at in-plane magnetic fields between 0 and 0.3 T. While this field is insufficient for the observation of Zeeman effect, it is enough to allow for penetration of vortices whose spectroscopic signature overwhelm any other sub-gap features.²²

To overcome this issue, we recall that few layer NbSe₂ has strong spin-orbit coupling, thus application of in-plane magnetic fields has negligible effect on the spectrum of such superconductors.²¹ Figure 2b shows the spectrum of Device 1, consisting of a tunnel junction into a 4 layer NbSe₂ flake, at in-plane magnetic fields ranging between 0 and 2.5 T. While the major features of the superconducting gap seem almost untouched by the field, the sub-gap spectrum changes significantly, as seen in Figure 2c which follows the evolution of the sub-gap spectrum of Device 1 with in-plane magnetic field. It is clear that the two symmetric sub-gap peaks split. The black traces fit the peak position according to a Zeeman energy with a g factor of 1.3. This observation, of splitting of the sub-gap peaks, repeats itself in all of the devices measured with g factors in the range of 1.3 to 2 (see supplementary information for sub-gap spectra of all of the devices measured).

This observation lends support to the claim that the zero field ground state of the proximitized dot is the singlet state. This was previously observed in quantum dots formed at the edges of nano-wires and carbon nano-tubes, with careful control over E_0 using dielectric gate. Compared with these systems, the proximitized dots formed in the vdW barriers tend to have a singlet ground-state, which points to small charging energy or to E_0 in the close vicinity of the Fermi energy. Furthermore, the observed magnitude of the g factor points to atomic defect, rather than a large quantum dot with an internal band structure that

re-normalizes g . For such an atomic defect, the broken inversion symmetry that leads to Ising spin-orbit coupling is of no importance. Thus, the spin orientation of the electrons on the dot are free to interact with the in-plane magnetic field.

When the Zeeman energy equals the zero field ξ , a degeneracy between the singlet and the lower energy doublet state occurs, giving rise to a zero energy conductance peak. Further increase of the magnetic field beyond this crossover field, leads to a shift of the ground state to the lower doublet state, a crossover whose spectroscopic signature is the disappearance of the higher energy split peaks.⁹ This is accompanied by crossing of the lower energy split peaks. Since the conduction in the junctions reported here consists of both tunneling through the quantum dot and tunneling directly between the normal metal and the superconductor, the higher energy peaks tend to merge with the above-gap conduction, thus hindering the observation of the former spectroscopic signal. The latter signal – crossing of the split peaks at zero energy – was evident in many of the measured devices (supplementary figure 2).

Zero bias conductance peaks (ZBCP)

Figure 3 shows the differential conductance (panels a,c) and sub-gap conductance (panels b,d) of Devices 3 and 4 respectively. In both devices a stable zero bias peak is formed at fields higher than the crossover field. This feature is stable for approximately 2.5 T, much higher than expected from spectral width of the sub-gap peaks. While in Device 3, the ZBCP is merged with the increasing background conductance beyond 3.5 T, in Device 4 the ZBCP splits at 4.5 T, only to reappear at 6.5 T.

ABS pinning to zero energy, beyond some critical in-plane field, is a feature repeatedly seen in proximitized nanowires.^{15,16,24} While such ZBCPs are often associated with Majorana fermions which appear due to non-trivial topology of the superconducting state, recent experimental²⁵ and theoretical¹⁸⁻²⁰ studies point to trivial origins of zero energy pinning, calling for extra scrutiny of such results. A different source of zero bias peaks, originating in coupling between the quantum dot and the superconductor, has also been reported in

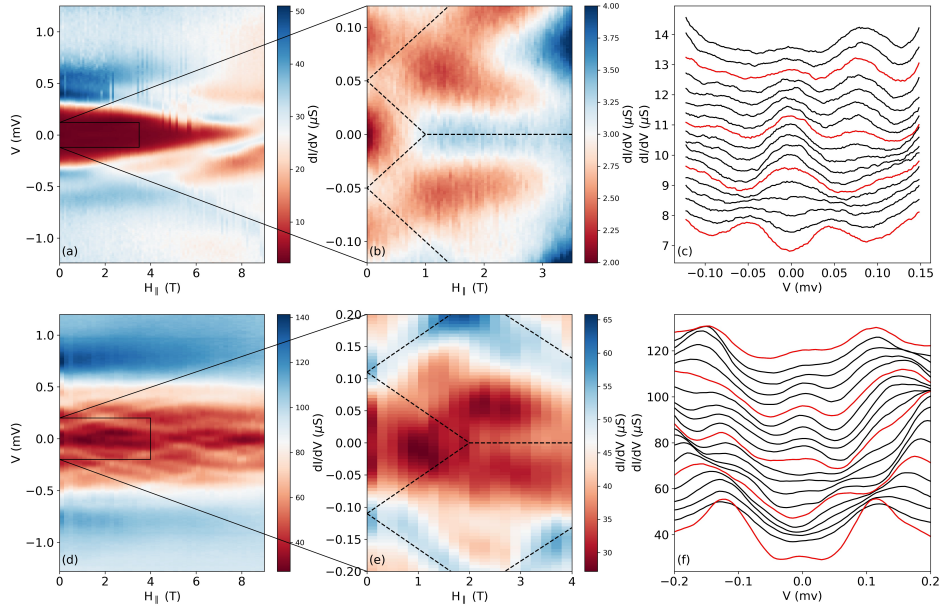


Figure 3: **Formation of zero energy states:** **a.** Color map of the sub-gap conductance of Device 3 with increasing in-plane magnetic field. **b.** Close up on the sub-gap region showing the formation of a stable zero bias peak. **c.** Shifted differential conductance curves from the sub-gap region of Device 3, the curves are shown at intervals of 0.2 T. Red curves are shown at intervals of 1 T. **d,e, f** Same for Device 4

proximitized nanowires.^{10,26} In what follows, we discuss alternative interpretations for the emergence of topologically trivial ZBCPs, in the NIS van der Waals system.

In principle, the system discussed here possesses the required ingredients for the formation of topological superconductivity that breaks time reversal symmetry and Majorana bound states: superconductivity, strong spin orbit coupling, and magnetic field which is applied perpendicular to the direction of the SOC. Formation of topological superconductivity is unlikely, as topological systems require the proximitized region to be large in at least a single dimension, to enable the formation of edge states. Since the sub-gap features reported here are in all likelihood associated with atomic scale quantum dots, as evident in the observed low g factor, we can rule out the topological origin of the stable ZBCP that is discussed in the context of nanowires.^{13,14} The combination of superconductivity, strong spin-orbit coupling and Zeeman field can form trivial nearly zero energy bound states in quantum dots, as recently shown in refs.^{18,19} There, a non superconducting quantum dot, in contact with a BCS superconductor, was theoretically shown to host such bound states when a magnetic field crosses a threshold, determined by the superconducting gap and the strength of the SOC. While the details of the discussed model and our van der Waals system are different, we believe that the phenomenon of pinning to zero bias is general. We study here a quantum dot embedded in a semi-conducting barrier that hosts a strong intrinsic Ising SOC in addition to Rashba SOC, in proximity to an ultra-thin Ising superconductor. This special type of proximitized quantum dot calls for further theoretical modelling.

A different possibility for the formation of zero bias peaks comes from the Kondo effect. It was shown that the ground state of a quantum dot coupled both to a superconductor and to a normal metal can be either the doublet or superconducting singlet as discussed, or a Kondo singlet that involves a superposition between the electrons in the dot and the electrons in the normal lead.¹⁰ Application of magnetic field can induce a SC singlet to Kondo singlet transition as a result of reduction in the magnitude of the superconductor order parameter or filling of the SC gap.²⁶ Kondo peaks, however, are stable only in magnetic fields smaller

than the Kondo temperature T_K , in which the Kondo resonance becomes apparent. Beyond such small fields, the Kondo degeneracy splits.⁸ Such splitting is not observed here.

Furthermore, the actual reduction in the magnitude of the superconducting gap can pin the excitation energy of the dot to zero by level repulsion.¹⁰ Few layer NbSe₂ is very resilient to the application of in-plane field. In fields of the range reported in this work, the superconducting gap hardly changes,²² rendering both mechanisms - Kondo or repulsion from the gap - implausible.

Conclusions

In summary, we show that vdW tunnel junctions using TMD barriers may serve as a platform to study the proximity between quantum dots and superconductors. This platform is set in the extreme limit of quantum dots whose dimensions are on the atomic scale, and also in the presence of a strong Ising spin orbit coupling. Our results suggest that the zero field ground state of such dots is analogous to the BCS singlet state, which can be tuned by the application of in-plane magnetic field. Finally, the formation of stable zero bias spectral features at finite magnetic fields calls for further theoretical investigation.

Acknowledgements

The authors are thankful for fruitful discussions with Y. Oreg and D. Loss. The authors are also thankful for A. Zalic, A. Vakahi and S. Remennik for TEM and SEM imaging. This work was funded by a Maimondes-Israel grant from the Israeli-French High Council for Scientific & Technological Research, an ANR JCJC grant (SPINOES) from the French Agence Nationale de Recherche, a European Research Council Starting Grant (No. 637298, TUNNEL), and Israeli Science Foundation grant 1363/15. T.D. is grateful to the Azrieli Foundation for an Azrieli Fellowship.

Author contributions

T.D. fabricated the devices. C.Q.H.L., T.D. and M.A. performed the measurements. All authors contributed to data analysis and the writing of the manuscript.

Competing financial interests

The authors declare no competing financial interests.

References

- (1) De Franceschi, S.; Kouwenhoven, L.; Schönberger, C.; Wernsdorfer, W. Hybrid superconductor–quantum dot devices. *Nature Nanotechnology* **2010**, *5*, 703–711.
- (2) Fazio, R.; Raimondi, R. Resonant Andreev Tunneling in Strongly Interacting Quantum Dots. *Physical Review Letters* **1998**, *80*, 2913–2916.
- (3) Clerk, A. A.; Ambegaokar, V.; Hershfield, S. Andreev scattering and the Kondo effect. *Physical Review B* **2000**, *61*, 3555–3562.
- (4) Bauer, J.; Oguri, A.; Hewson, A. C. Spectral properties of locally correlated electrons in a Bardeen–Cooper–Schrieffer superconductor. *Journal of Physics: Condensed Matter* **2007**, *19*, 486211–20.
- (5) Governale, M.; Pala, M. G.; König, J. Real-time diagrammatic approach to transport through interacting quantum dots with normal and superconducting leads. *Physical Review B* **2008**, *77*, 659–14.
- (6) Gräber, M. R.; Nussbaumer, T.; Belzig, W.; Schönberger, C. Quantum dot coupled to a normal and a superconducting lead. *Nanotechnology* **2004**, *15*, S479–S482.

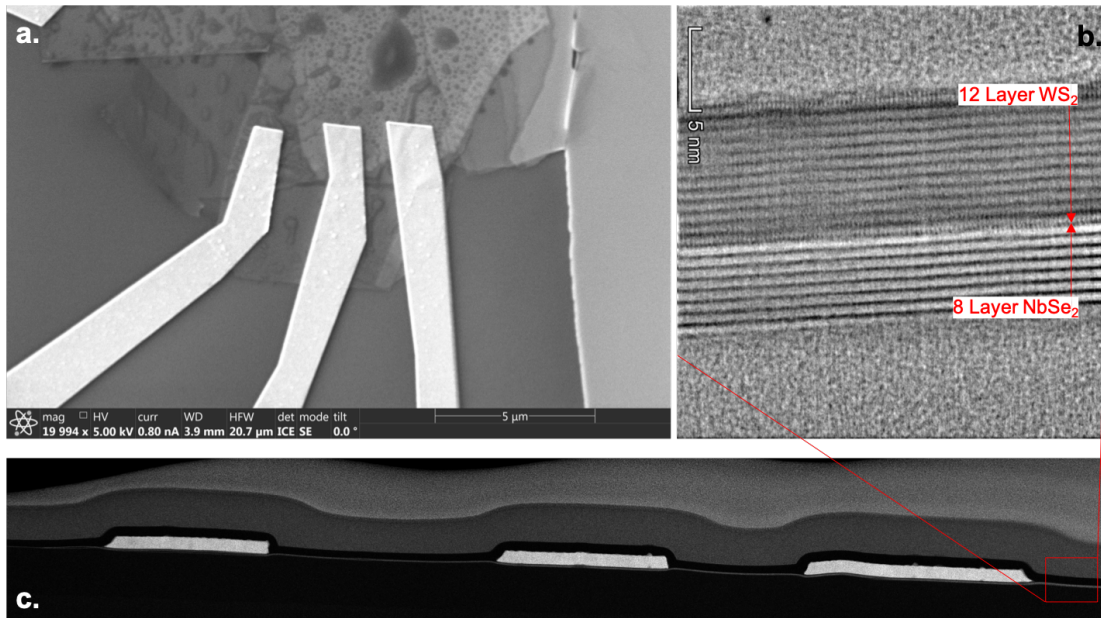
- (7) Pillet, J.-D.; Joyez, P.; Žitko, R.; Goffman, M. F. Tunneling spectroscopy of a single quantum dot coupled to a superconductor: From Kondo ridge to Andreev bound states. *Physical Review B* **2013**, *88*, 045101–6.
- (8) Deacon, R. S.; Tanaka, Y.; Oiwa, A.; Sakano, R.; Yoshida, K.; Shibata, K.; Hirakawa, K.; Tarucha, S. Kondo-enhanced Andreev transport in single self-assembled InAs quantum dots contacted with normal and superconducting leads. *Physical Review B* **2010**, *81*, 659–4.
- (9) Lee, E. J. H.; Jiang, X.; Houzet, M.; Aguado, R.; Lieber, C. M.; De Franceschi, S. Spin-resolved Andreev levels and parity crossings in hybrid superconductor–semiconductor nanostructures. *Nature Nanotechnology* **2014**, *9*, 79–84.
- (10) Jellinggaard, A.; Grove-Rasmussen, K.; Madsen, M. H.; Nygård, J. Tuning Yu-Shiba-Rusinov states in a quantum dot. *Physical Review B* **2016**, *94*, 85–8.
- (11) Meng, T.; Florens, S.; Simon, P. Self-consistent description of Andreev bound states in Josephson quantum dot devices. *Physical Review B* **2009**, *79*, 659–10.
- (12) Deacon, R. S.; Tanaka, Y.; Oiwa, A.; Sakano, R.; Yoshida, K.; Shibata, K.; Hirakawa, K.; Tarucha, S. Tunneling Spectroscopy of Andreev Energy Levels in a Quantum Dot Coupled to a Superconductor. *Physical review letters* **2010**, *104*, 076805–4.
- (13) Oreg, Y.; Refael, G.; von Oppen, F. Helical Liquids and Majorana Bound States in Quantum Wires. *Physical Review Letters* **2010**, *105*, 177002.
- (14) Lutchyn, R. M.; Sau, J. D.; Das Sarma, S. Majorana Fermions and a Topological Phase Transition in Semiconductor-Superconductor Heterostructures. *Physical review letters* **2010**, *105*, 077001–4.
- (15) Mourik, V.; Zuo, K.; Frolov, S. M.; Plissard, S. R.; Bakkers, E. P. a. M.; Kouwen-

- hoven, L. P. Signatures of Majorana fermions in hybrid superconductor-semiconductor nanowire devices. *Science* **2012**, *336*, 1003–1007.
- (16) Deng, M. T.; Vaitiekėnas, S.; Hansen, E. B.; Danon, J.; Leijnse, M.; Flensberg, K.; Nygård, J.; Krogstrup, P.; Marcus, C. M. Majorana bound state in a coupled quantum-dot hybrid-nanowire system. *Science* **2016**, *354*, 1557–1562.
- (17) Das, A.; Ronen, Y.; Most, Y.; Oreg, Y.; Heiblum, M.; Shtrikman, H. Zero-bias peaks and splitting in an Al–InAs nanowire topological superconductor as a signature of Majorana fermions. *Nature Physics* **2012**, *8*, 887–895.
- (18) Reeg, C.; Dmytruk, O.; Chevallier, D.; Loss, D.; Klinovaja, J. Zero-energy Andreev bound states from quantum dots in proximitized Rashba nanowires. *Physical Review B* **2018**, *98*, 1–12.
- (19) Liu, C.-X.; Sau, J. D.; Stanescu, T. D.; Das Sarma, S. Andreev bound states versus Majorana bound states in quantum dot-nanowire-superconductor hybrid structures: Trivial versus topological zero-bias conductance peaks. *Physical Review B* **2017**, *96*.
- (20) Avila, J.; Peñaranda, F.; Prada, E.; San-Jose, P.; Aguado, R. Non-Hermitian topology: a unifying framework for the Andreev versus Majorana states controversy. *arXiv:1807.04677* **2018**,
- (21) Dvir, T.; Aprili, M.; Quay, C. H. L.; Steinberg, H. Tunneling into the Vortex State of NbSe₂ with van der Waals Junctions. *Nano Letters* **2018**, *18*, 7845–7850.
- (22) Dvir, T.; Masee, F.; Attias, L.; Khodas, M.; Aprili, M.; Quay, C. H. L.; Steinberg, H. Spectroscopy of bulk and few-layer superconducting NbSe₂ with van der Waals tunnel junctions. *Nature Communications* **2018**, *9*, 598.
- (23) Barański, J.; Domański, T. In-gap states of a quantum dot coupled between a normal

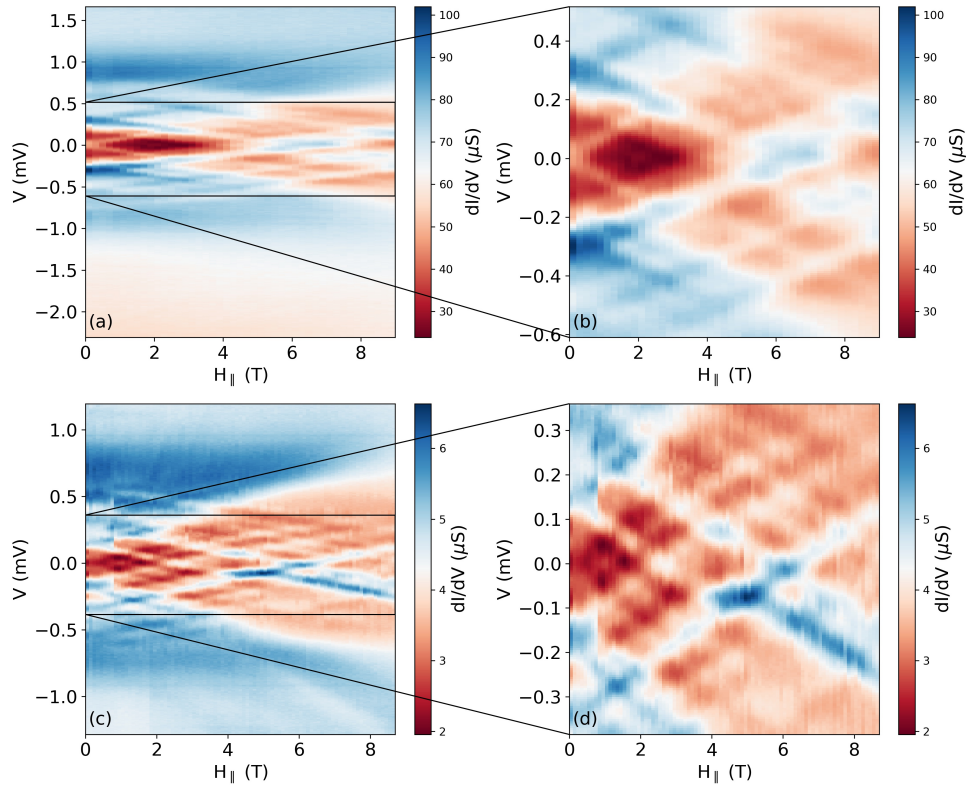
and a superconducting lead. *Journal of Physics: Condensed Matter* **2013**, *25*, 435305–10.

- (24) Zhang, H. et al. Quantized Majorana conductance. *Nature* **2018**, *556*, 74–79.
- (25) Chen, J.; Woods, B.; Yu, P.; Hoeschele, M.; Car, D.; Plissard, S.; Bakkers, E.; Stanescu, T.; Frolov, S. Ubiquitous non-Majorana Zero-Bias Conductance Peaks in Nanowire Devices. *arXiv:1902.02773* **2019**,
- (26) Lee, E. J. H.; Jiang, X.; Aguado, R.; Katsaros, G.; Lieber, C. M.; De Franceschi, S. Zero-Bias Anomaly in a Nanowire Quantum Dot Coupled to Superconductors. *Physical review letters* **2012**, *109*, 659–5.

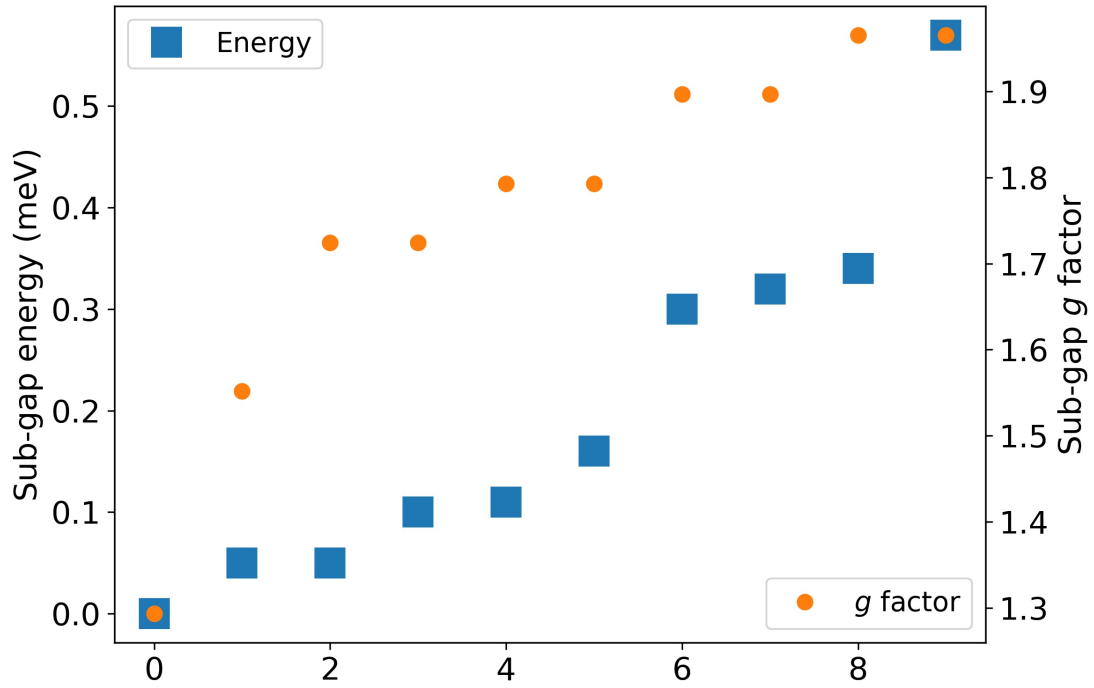
Supplemental Materials: Zeeman tunability of Andreev bound states in van-der-Waals tunnel barriers



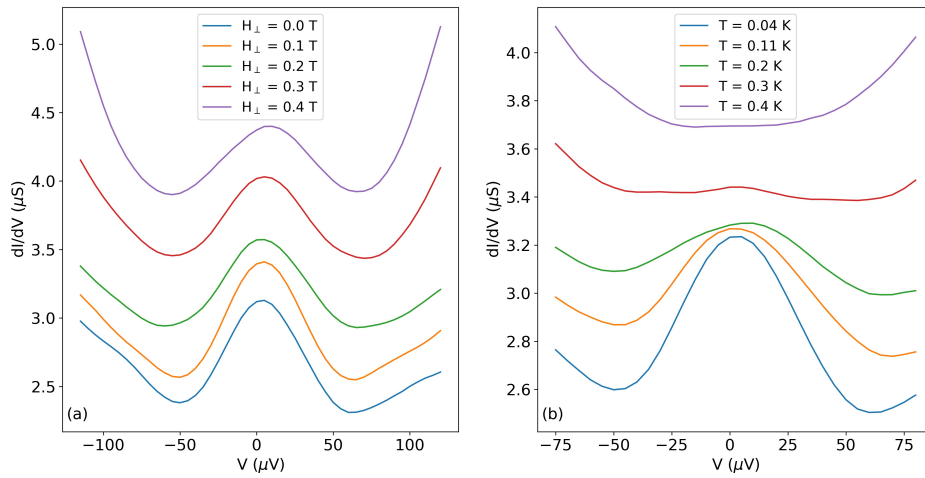
Supplementary Figure S1: Typical device interface: a. SEM imaging of Device 5. b., c. Cross section TEM along a line cut of Device 5.



Supplementary Figure S2: Additional devices: **a** Color map of the sub-gap conductance of Device 6 with increasing in-plane magnetic field. **b.** Zoom in on the sub-gap region showing the linear dispersion of the energy of the sub-gap peaks with magnetic field. **c,d** Same for Device 7



Supplementary Figure S3: Multiple dots compilation Sub-gap zero field energies and g factor for all measured dots.



Supplementary Figure S4: ZBCP of Device 3: **a.** Perpendicular field dependence of the ZBCP of Device 3. **b.** Temperature dependence of the ZBCP of Device 3.